A Multiscale Study of High Performance Double-Walled Nanotube–Polymer Fibers

Mohammad Naraghi,[†,§] Tobin Filleter,[†,§] Alexander Moravsky,[‡] Mark Locascio,[†] Raouf O. Loutfy,[‡] and Horacio D. Espinosa[†,*]

[†]Department of Mechanical Engineering, Northwestern University, 2145 Sheridan Road, Evanston, Illinois 60208, United States, and [‡]MER Corporation, 7960 South Kolb Road, Tucson, Arizona 85706, United States. [§]These authors contributed equally to this work.

ABSTRACT The superior mechanical behavior of carbon nanotubes (CNT) and their electrical and thermal functionalities has motivated researchers to exploit them as building blocks to develop advanced materials. Here, we demonstrate high performance double-walled nanotube (DWNT)–polymer composite yarns formed by twisting and stretching of ribbons of randomly oriented bundles of DWNTs thinly coated with polymeric organic compounds. A multiscale *in situ* scanning electron microscopy experimental approach was implemented to investigate the mechanical performance of yarns and isolated DWNT bundles with and without polymer coatings. DWNT–polymer yarns exhibited significant ductility of ~20%, with energy-to-failure of as high as ~100 J g^{-1}, superior to previously reported CNT-based yarns. The enhanced ductility is not at the expense of strength, as yarns exhibited strength as high as ~1.4 GPa. In addition, the significance of twisting on the densification of yarns and corresponding enhancement in the lateral interactions between bundles is identified. Experiments at nanometer and macroscopic length scales on DWNT–polymer yarns and bundles further enabled quantification of energy dissipation/storage mechanisms in the yarns during axial deformations. We demonstrate that while isolated DWNT bundles are capable of storing/dissipating up to ~500 J g^{-1} at failure, unoptimal load transfer between individual bundles prevents the stress build up in the yarns required for considerable energy storage at the bundle level. By contrast, through polymer lateral interactions, a much better performance is obtained with the majority of energy dissipated at failure being contributed by the interactions between the polymer coating and the DWNTs as compared to the direct van der Waals interactions between bundles.

KEYWORDS: carbon nanotubes bundles · carbon nanotubes yarns · energy-to-failure · nanocomposites · *in situ* mechanical testing

The study of natural materials provides great insight into the hierarchical design of structures to achieve remarkable mechanical performance with both high strength and robustness. The superior mechanical performance found in nature is in contrast to common engineering materials, such as ceramics and metals, in which there is a trade-off between strength and toughness.[9,13–17] Hierarchical designs in nature, such as in bones and proteins, span a wide range of length scales in which the materials are known to be significantly robust and insensitive to flaws with toughening mechanisms present across nanoscale, mesoscale, and macroscopic lengths.[3,16,18–21] The hierarchy in nature has motivated attempts to mimic natural structures toward the development of high strength/toughness materials.[18,22–27]

One promising building block to synthesize biomimetic hierarchical structures is carbon nanotubes (CNT), which in their pristine form offer significant strength and modulus, in the order of 100 GPa and 1 TPa, respectively.[28–30] In addition, due to their high thermal stability and electrical properties, they can add thermal and electrical functionalities to the constituting structures.[1,31–33]

However, recent attempts to incorporate CNTs into hierarchical structures point to the inefficient integrity between the neighboring CNTs and/or the CNTs and the other constituents of the macrostructures. As a result, the superior mechanical properties of CNTs are only marginally utilized. Windle *et al.* have devised and implemented an *in situ* chemical vapor deposition (CVD) spinning method to obtain continuous CNT yarns from CVD grown CNT aerogels.[1,2,34] The stretching of the low density aerogels of CNTs with low entanglement generated inside the CVD reactor allowed for significant alignment of the CNTs leading to high mechanical performance of the yarns. Using *in situ* CVD spinning technology, the Windle group was able to fabricate CNT yarns with specific strengths as high as ~9.5 Ntex^{-1} at small gage lengths of ~1 mm. Defects resulted in a substantial reduction of specific strength to ~1 Ntex^{-1} at 20 mm gage length and energy-to-failures to ~30–65 J g^{-1}.[2,9,35] These values are comparable to the properties of high performance fibers such as Kevlar as listed in ref 2. However, the yarns fabricated by this method are not highly uniform in diameter, which can potentially induce stress

*Address correspondence to espinosa@northwestern.edu.

Received for review June 21, 2010 and accepted October 19, 2010.

Published online October 26, 2010.
10.1021/nn101404u

concentrations and cause premature failure.[10] In addition, it has been suggested that the relatively large diameter of the CNTs and their consequent collapsed structure yields enhanced mechanical performance; however, further understanding of the role of van der Waals interactions is still needed to elucidate this enhancement.[2,34−36]

Another approach toward developing high performance structures from CNTs was proposed by Baughman *et al.*[37] which included extracting CNT yarns from forests of CNTs by the introduction of twist to the CNTs. A high degree of alignment was achieved by this method. The strength and energy-to-failure of their samples was *ca.* 0.3−0.6 Ntex^{-1} and 14−20 J g^{-1}, respectively.[3,38] This process was further enhanced by Liu *et al.*, in which yarn spinning was performed by a combination of twisting and solvent assisted shrinking of the CNTs from CNT forests. It was demonstrated that shrinking and twisting enhances the mechanical performance of the yarns potentially due to the increased interaction between CNTs.[39] Moreover, Baughman *et al.*[3] have infiltrated the spun yarns with polymers such as polyvinyl alcohol (PVA) to enhance the interactions between CNTs and the mechanical performance of the yarns. These attempts have led to slightly stronger yarns at the cost of a reduction in ductility and consequently lower energy-to-failure. Other approaches such as drawing yarns from CNTs solutions and gels have also been introduced, through which CNT-based composites with high concentration of CNTs are fabricated.[1,4,6] These methods were primarily implemented to allow for more interactions between CNTs through polymer molecule intermediaries, potentially increasing the yarns toughness and strength. Despite the significant improvements in recent years toward developing CNT-based yarns, these examples all point to the fact that mechanical properties of these structures, such as their strength and energy-to-failure, remain significantly lower than those exhibited by CNTs.

While the most significant contributing factors in the relatively poor mechanical performance of CNT-based macrostructures have been identified as inferior hierarchical designs and low load transfer between CNTs, a more detailed fundamental understanding of load bearing mechanisms and energy storage/dissipation mechanisms is necessary to bridge the gap between the mechanical properties of these macroscale samples and their nanoscale constituents. A number of fundamental studies on individual CNTs and CNT bundles have begun to develop this desired fundamental understanding. Ruoff *et al.* performed *in situ* scanning electron miscroscopy (SEM) tensile tests of both multiwalled nanotubes (MWNTs) and single-walled nanotube (SWNT) bundles, experimentally demonstrating the exceptional mechanical properties of individual tubes, as well as identifying weak shear interactions between adjacent MWNT shells.[40,41] Through *in situ* transmission electron microscopy (TEM) testing, our group has experimentally measured, for the first time, CNT modulus and strength consistent with quantum mechanical predictions.[29] Moreover, the advantages of covalently cross-linking inner shells of MWNTs as well as the SWNT within bundles to improve load transfer between shells have also been demonstrated.[28,29,42]

In the current study, in order to develop a fundamental understanding of the effect of interactions between CNTs on the mechanical performance of CNT-based yarns, we have carried out a multiscale experimental approach to quantify the effect of shear interactions *via* polymer cross-linking of CNTs. Here, CNT-based yarns were fabricated from chemical vapor deposition (CVD) grown double-walled nanotube (DWNT) mats. The mats were composed of bundled DWNTs, coated *in situ* with approximately a monolayer of organic polymer during the CVD process. DWNTs in particular have the advantage of a higher density of load bearing graphitic shells as compared to larger MWNTs. The organic layer has been found to substantially enhance the interactions between CNTs, thus improving the mechanical performance of the yarns. Following thermal treatments, the polymer coating was removed, considerably altering the interactions between adjacent CNTs and providing a comparison in mechanical properties. We have adopted a unique approach in which we study both the macroscopic yarns as well as their nanoscale constituents, individual DWNT bundles, and we use the results of the latter to interpret the former. This approach allows an unambiguous comparison of the material properties on multiple length scales within the hierarchical network, leading to fundamental insights into the relative effectiveness of different load transfer mechanisms in CNT-based materials. Our multiscale experimental approach is composed of *in situ* SEM nanoscale experiments on individual bundles and *in situ* SEM tension tests on macroscale yarns, in which the mechanical performance of the bundles and yarns, their modes of failure, and the correspondence between the two scales are identified. Through our multiscale approach, we demonstrate that an enhancement in lateral interactions between CNT bundles as a result of polymer cross-linking has significantly improved the mechanical performance of the DWNT-based yarns.

RESULTS

DWNT yarns were fabricated by spinning DWNT mats produced by MER Corp. in a CVD process by using a floating catalyst system based on ferrocene as the catalyst precursor and ethyl alcohol as a hydrocarbon feedstock. The mats are composed of an interwoven network of DWNT bundles. Figure 1 shows the hierarchy of the yarn structure down to individual DWNT

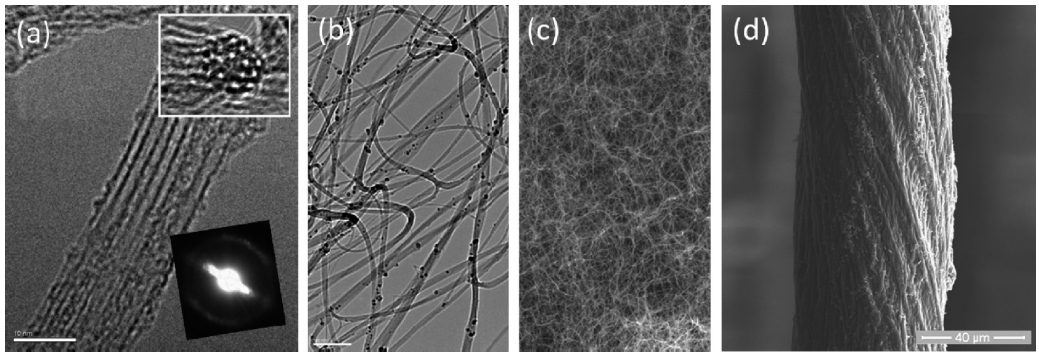

Figure 1. Hierarchy of DWNT mat material. (a) Individual DWNT bundle. Scale bar: 10 nm. Insets: (top) crossection of individual bundle; (bottom) nanodiffraction pattern of an individual bundle. (b) TEM image of interconnected DWNT bundles including Fe particles. Scale bar: 100 nm. (c) SEM image of DWNT mat. (d) SEM image of a DWNT yarn.

bundles. Each bundle within the mat is composed of up to tens of hexagonally close-packed DWNTs. These DWNT building blocks have an outer diameter of ~2.2 nm, determined from Raman spectra breathing modes (not shown), and a spacing of ~2.5 nm between adjacent DWNTs within bundles, measured from high resolution TEM images. Nanodiffraction patterns of individual bundles reveal variation in the orientation of the CNTs lattice with respect to the electron beam in TEM resulting in continuous bands in the diffraction patterns (see Figure 1a). This can either indicate a variation in chiral angle for CNTs within the bundles or misalignment with respect to the bundle axis.[43]

In combination with other analytical techniques such as FTIR, the thermogravimetric analysis (TGA) of the as-produced DWNT mats in air and argon (Figure 2) enables identification and quantitative determination of the contents of the mat components that include DWNTs, organic compounds, iron, amorphous and graphitized carbon. When organic compounds are volatized by heating (Figure 2), they turn into a multicomponent gas mixture that is dominated by the molecules of substituted acrylic acid esters with the general formula R′CH═CR′′COOR, where R, R′ and R′′ stand for hydrogen, alkyl, alkenyl, and aryl groups in various combinations, as demonstrated by mass-spectrometric (MS) analysis.

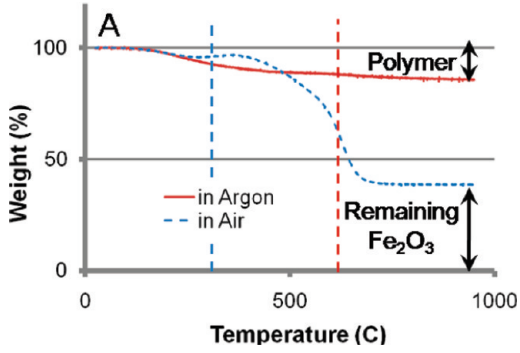

Figure 2. Heat treatment to remove polymer coating. TGA spectra in argon and air at 20 °C min^{-1} demonstrating the removal of the majority of the polymer coating in argon at 600 °C.

Organic compounds can also be extracted from DWNT mats by applying a set of common solvents to the mat. FTIR and HPLC/UV analyses confirm the dominance of molecules of substituted acrylates in these extracts. Polyacrylates undergo scission into monomers upon thermal decomposition and dissolution. The polyacrylate layer is formed in the CVD reactor from the same acrylate monomers identified above. The gas phase in the nanotube synthesis consists of hydrogen, ethylene, acetylene, carbon monoxide, methane, and water vapor mixture, which is also well suited for the synthesis of acrylic acid derivatives. The acrylate monomer synthesis takes place in the moderately hot zone of the reactor after the nanotube synthesis is completed and is likely catalyzed by the surface of nanotubes, where the polymerization is also occurring and the resulting polyacrylate layer eventually resides. Therefore, based on the data above and electron microscopy observations it is speculated that the organic compounds in the as-produced DWNT mat exist as a thin polymeric layer that coat the DWNT bundles, which may also be present on the inner tubes.

As demonstrated in the TGA analysis, Figure 2, the majority of the polymer coating can be vaporized and removed at a temperature of 600 °C in argon (vertical red line). Beyond 600−700 °C, little weight change is observed in Ar. Moreover, TGA experiments in air demonstrate a yarn-mat mass loss which reaches a local plateau at *ca.* 250−400 °C (vertical blue line in Figure 2), attributed to the burning of the amorphous carbon and polymeric coatings. The upper limit in this temperature range points to the onset of the burning of the SWNT. These results specifically identify the heat treatments required to remove the polymer coating without modifying the sp^2 bonding in DWNTs both in argon and in air.[44,45] Further heating of the sample to higher temperatures in air shows a rapid weight loss starting at ~450 °C and continuing to 700 °C, during which DWNTs and iron catalysts are burned. The TGA experiments in Ar point to the presence of ~14.5 wt % polymer coating in the yarns, while the

TGA experiments in air reveal the presence of ~35 wt % of Fe_2O_3 residues which translates to ~24.5 wt % of Fe in the as-fabricated mats.

On the basis of these findings, an argon−air heat treatment was applied to the as-fabricated yarns and mats (pristine samples) which contain the polymer coatings to produce DWNT yarn and mats without the cross-linking polymer coating (heat-treated samples) in order to study the effect of polymer coating on the mechanical behavior of yarns and bundles. More details of the heat treatment are presented in the experimental section.

Mechanical Behavior of DWNT Yarns. *In-situ* SEM mechanical characterization of CNT-based yarns was carried out using a tensile testing stage, allowing for simultaneous measurement of the mechanical behavior of samples and identification of mechanisms of deformation and failure of the material.

Since both enhanced mechanical behavior and lightweight are desired for most advanced structural materials, here we have calculated the mechanical properties of yarns in terms of specific properties such as specific strength (ratio of yarn strength in units of stress to density) and energy-to-failure per unit weight. In addition, for comparisons with other structural materials and with individual DWNT bundles, we also report our measurements of the yarns mechanical properties based on estimates of the yarns cross section.

To calculate the yarns effective diameter, the cross-sectional area of DWNTs in the yarns is determined from the mass of CNTs within the sample and the density of CNT bundles with a nominal density $\rho_{bundle} \approx 1.575$ g/cm^3 as estimated in the Supporting Information. The effective cross section of each yarn, by excluding the volume of the pores between bundles, can be estimated as

$$A_{effective} = \frac{\lambda}{\rho_{bundle}} \quad (1)$$

where λ is the linear density of the CNTs in the yarns. Since iron particles do not contribute to the load bearing in the yarns, they are excluded in the effective area measurements, as suggested by Motta *et al.*[10] The effective diameter of the yarns is then calculated as the diameter of a yarn with a circular cross section with an area of $A_{effective}$.

A sample of the specific stress-engineering strain curve of a DWNT-based yarn obtained in this study is shown in Figure 3a. In this case, the yarn was fabricated from a $^1/_8$ in. wide ribbon of a DWNT mat, and the sample gage length was ~1 cm. The sample failed at a specific stress of ~0.8 N/tex, which translates to ~1.4 GPa. It also demonstrates a large ductility of ~20% engineering strain. The energy-to-failure of this specific sample is ~100 J g^{-1} of DWNTs weight. Subsequent to the removal of the inherent polymer coating, the specific strength slightly increases to ~1.0 N/tex (equivalent to ~1.6 GPa), while the ductility and energy-to-failure substantially drop, Figure 3a. The results shown in Figure 3a are typical of the yarns made out of ribbons with the same ribbon width ($^1/_8$ in.), as will be discussed further in this section.

The fractography of the yarns points to an interesting aspect of their morphology. From the SEM images of the surfaces of the yarns, for instance Figure 1d, we see that the yarns may resemble a continuous filament-like structure fabricated through twisting a series of filaments together,[46] SEM images of the fracture surface instead reveal their true structure. As shown in Figure 3b, the filament-like structures observed on the surface are wrinkled layers of the original ribbon used to fabricate the yarn. This morphology is most likely a consequence of successive buckling of the mat during spinning which results in ridges similar to those formed in thin cylinders after being twisted to the postbuckling regime.[47,48] It is important to note that the polymer coating binds the wrinkled layers of the yarn, thus enhancing its structural stability and integrity. This feature becomes apparent when monitoring the structure of heat-treated yarns (no polymer coating) in which the stacked wrinkled layers of the mat are partially unfolded at several locations due to the loss of binding polymeric molecules, Figure 3c. It is however to be noted that even in this case, van der Waals interactions between the neighboring mats brings a degree of structural stability to the yarns.

The *in situ* SEM experiments also reveal the mechanisms of deformation of the yarns. As shown in Figure 3d−f, the axial deformation of the pristine yarns (before heat treatment) is accompanied by aligning the ridges of the buckled wrinkles with the loading direction. As the yarn is stretched from an undeformed configuration to an average engineering strain of ~14% (cross head displacement normalized by the initial yarn length), the angle between the wrinkles' ridges and the axis of the yarn is reduced from ~23° to ~10.3°. In addition, sample stretching is accompanied by the twisting, realized for instance by tracking the motion of the particles on the surface of the yarn in Figure 3d−f. This twist of the yarns during axial deformations demonstrates the development of a torque during axial loading. This mode of deformation is reminiscent of the mechanical behavior of the filament yarns under axial load when the constitutive filaments have the same layout (twisted in the same direction).[46] The development of this moment in the yarn upon axial loading can be explained by the significantly higher stiffness of the wrinkles in the direction of the ridges compared to the lateral direction (direction of compressive stress during buckling) along which due to buckling they have substantially lost their load bearing capability. As a result, the axial force on the yarn is carried by the wrinkles in the direction parallel to the ridges which makes a finite

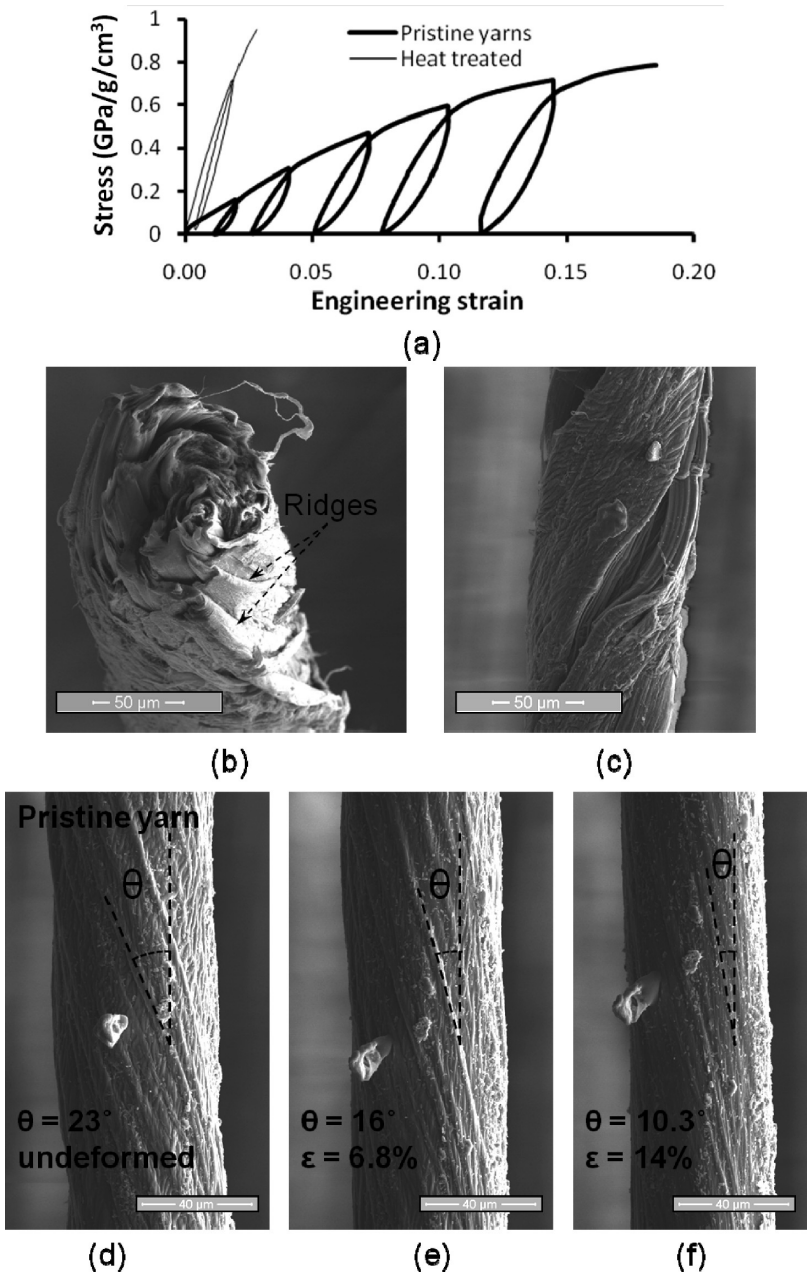

Figure 3. (a) Specific stress as a function of engineering strain in DWNT based yarns. (b) The post-mortem SEM images of the fractured surface of the yarns clearly points to the buckled structure of the mat formed during spinning. (c) SEM image of the heat-treated yarns. The removal of the polymer coating reduces the interaction between layers of the mat in the yarns causing partial unfolding. SEM images of a yarn during *in situ* SEM tension test at (d) zero load, (e) 6.8% eng. strain, and (f) 14% eng. strain.

angle with the yarn axis (~23° to ~10.3° in Figure 3), thus a net torque is induced on the sample. A consequence of the combined stretching and torsion on the yarn is the enhancement of lateral confinement during axial loading, and the very high Poisson ratio, noticed by significant shrinkage of the yarn diameter (~13% reduction in diameter in ~14% axial strain), shown in Figure 3d−f.

It is illustrative to estimate the material strain $\varepsilon_{material}$ by decomposing the total engineering strain $\varepsilon_{engineering}$ into two parts,[49] as follows:

$$\varepsilon_{engineering} = \underbrace{\left(\sqrt{\frac{1+q_0^2}{1+q^2}} - 1\right)}_{\text{Reorientation}} + \underbrace{\varepsilon_{Material}\sqrt{\frac{1+q_0^2}{1+q^2}}}_{\text{CNT network stretching}} \quad (2)$$

where $q_0 = \tan(\vartheta_0)$, $q = (1 + \varepsilon_{engineering}) \cdot \tan(\vartheta)$, and θ_0 and θ are the initial and current ridge angles. The first term on the right-hand side of this equation represents the yarn strain induced by the reorientation and tilting of the ridges toward the loading direction, while the second term represents the component of the true strain in the axial direction of the yarn.

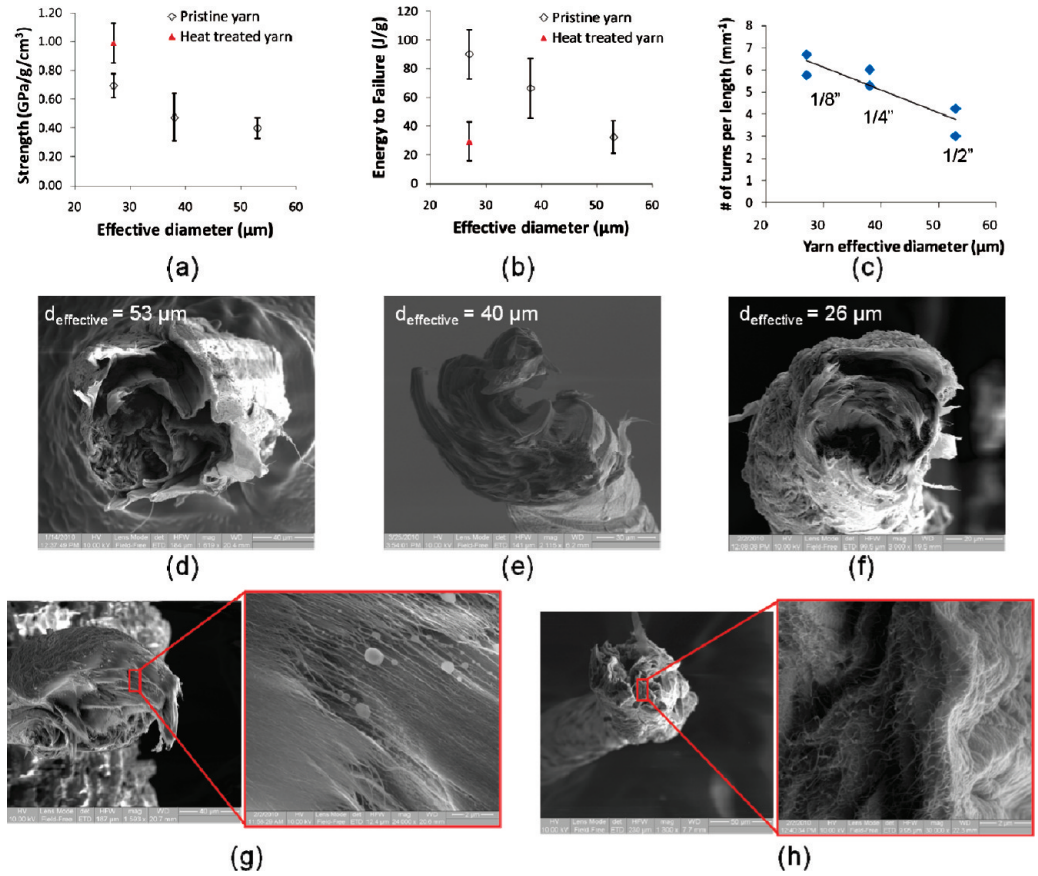

Figure 4. (a) Strength and (b) energy-to-failure as a function of diameter for the pristine and heat-treated yarns. (c) The spinability of the yarns as a function of yarn effective diameter, for each yarn diameter the corresponding ribbon width is shown on the plot. Postmortem SEM images of the cross section of the pristine yarns with an effective diameter of (d) 55, (e) 38, and (e) 27 μm. Postmortem SEM images of the cross section of the (g) pristine and (h) heat-treated yarns, pointing to the cooperative deformation of the bundles specific to the pristine yarns (g).

In this analysis, it is assumed that each yarn is composed of oriented fibrils making an initial angle of $\vartheta_0 \approx 23°$ with the axis of the undeformed yarn, Figure 3d. Hence, right before rupture we have $\theta \approx 10.3°$, $\varepsilon_{engineering} \approx 14\%$, and $\varepsilon_{material} \approx 6.3\%$. In other words, out of 14% overall strain measured in the sample, only about half will stretch the network of the bundles, while the rest of it tends to align the ridges with the loading direction and thus will transform the macroscopic structure of the yarns to a more compact structure (supported by the evident reduction in diameter during axial loading augmenting to a Poisson's ratio of *ca.* −0.8 to −0.9). Therefore, we speculate that the presence of the initial twist in the yarns has a positive effect on the strength by compressing the yarn laterally and increasing the interactions between bundles. Moreover, one may argue that the initial twist potentially increases the strength beyond the strength of the untwisted yarn. This can be hypothesized by considering the following two cases: a twisted yarn and yarn with no twist. In both cases, near failure, the ridges will be nearly parallel to the loading direction (consider Figure 3f for the first case). However, the former will benefit from the extra densification it will undergo during axial loading, which is absent in the latter, leading to more bundle−bundle interaction. However, this hypothesis cannot be verified experimentally since the twisting procedure is required to achieve strong yarns from the initially very fragile mats. Therefore, it is believed that the special morphology of the wrinkles of the yarns can enhance both the ductility and strength of the yarns, and as a consequence the energy-to-failure.

The specific strength and energy-to-failure of the pristine yarns (with inherent polymer coating) as a function of effective diameter are shown in Figure 4 panels a and b, respectively. Each point in these figures represents an average of a minimum of 3 measurements. The graphs point to a monotonic decrease of the mechanical properties of the yarns with effective diameter increase. As the effective diameter increases from 27 to 53 μm, the specific strength and energy-to-failure decrease from 0.70 ± 0.07 to 0.40 ± 0.07 $Ntex^{-1}$ (approximately from 1.4 ± 0.1 to 0.8 ± 0.1 GPa) and from 109 ± 17 to 38 ± 13 $J\,g^{-1}$, respectively. The origin of the enhanced mechanical performance of the thinner yarns is evident in the cross-sectional images of fractured yarns, Figure 4d−f. As shown in the figure, the thinner yarns have a more compact cross section (less porous) especially in the core of the yarn due to the higher twists imposed on narrower ribbons in the spinning

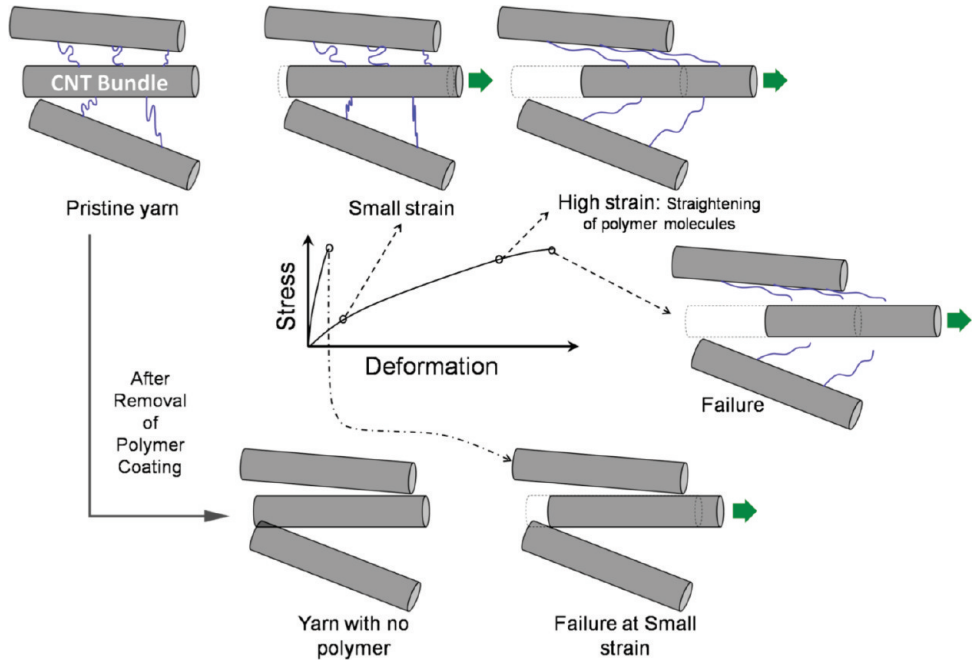

Figure 5. Schematic representation of the deformation of pristine yarns and the cooperative load bearing through polymer coating. Upon removal of the polymer, the network loses its ability to sustain large deformations. The cooperative deformation in the pristine yarns has a striking similarity with natural materials such as bone, in which a soft matrix (mainly composed of collagen) is reinforced with a stiff inorganic component (minerals platelets) to attain both high toughness and strength.[12] The mechanical functionality of the collagen matrix and mineral platelets in bone are similar to the functionalities of the inherent polymer coating and CNTs in our developed material system.

process. In other words, narrower ribbons of mats allows for a more uniform twist in different portions of the mat, resulting in a more compact yarn throughout the cross section. The higher amount of twist on narrower ribbons is quantified by the number of twists per unit length of the ribbons plotted as a function of the ribbon width in Figure 4c. Wider ribbons (thicker yarns) reach the critical force per unit width of the ribbons (80 mN mm^{-1}) at a smaller number of turns during spinning. This is due to the higher shear strains that develop during spinning on wider yarns at a given number of turns, which increases the stress in the yarn during spinning. The higher capability of narrower ribbons to be spun without failure allows for the development of a higher compactness, and thus it induces stronger interactions between the CNT bundles inside each yarn. This enhanced mechanical performance of yarns with higher twist has been previously predicted.[50]

Figure 3a and Figure 4a,b also point to the significant differences between the mechanical behavior of pristine (with inherent polymer coating) and heat-treated yarns. It is noteworthy to emphasize that the main distinction between the yarns before and after heat treatment is the amount of polymer content, which is significantly lower in the latter. As shown in Figure 3a, after the removal of polymer, the yarns appear to be significantly stiffer and more brittle. These differences in the mechanical behavior of the yarns point to the increased short-range interactions between bundles as a result of the removal of the polymer coating. The increased short-range interactions between bundles are motivated by the more compact structure of heat-treated yarns evidenced by ~15% shrinkage of their diameter as a result of heat treatment compared to the pristine ones. On the contrary, in the pristine yarns, the polymer coatings between the bundles increases the interbundle distances and acts as a plasticizer facilitating the mutual sliding of the bundles on each other especially at small deformations. As a result, the pristine yarns are significantly more compliant.

The contribution of the polymer coating to the overall deformation of the yarn is clearly evident in the differences observed between the fracture surfaces of the pristine yarns (Figure 4g) and heat-treated yarns (Figure 4h). In the former, the DWNT bundles deform cooperatively, and they slide significantly on the neighboring bundles during the test, while in the latter individual DWNT bundles pulled out resulting in a disordered and unaligned morphology. In other words, the load transfer between DWNT bundles *via* polymer molecule intermediaries significantly expands the fracture process zone in pristine yarns, allowing the material to dissipate more energy before failure.

Despite the initial low stiffness of the pristine yarns, their ultimate strength is only marginally affected by the removal of the polymer coating, Figure 4a. This observation suggests that despite the initial weak load transfer between bundles in the pristine yarns, where the interbundle interactions are governed by polymer

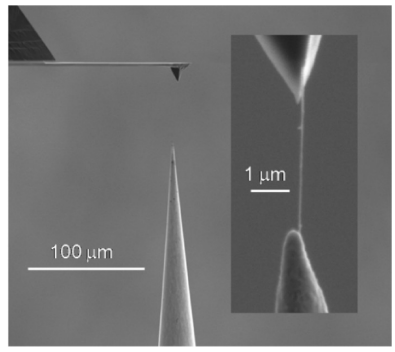

Figure 6. *In-situ* SEM tensile testing setup used for mechanical testing of DWNT bundles. (Inset) Isolated DWNT bundle attached between Si tip and nanomanipulator tip. The force is measured by the deflection of the Si tip.

molecules (initial low stiffness of pristine yarns), the shear interactions between bundles improve as a result of yarn axial stretching. In other words, at low strains, the interactions between bundles through polymeric molecules are low due to low elasticity of coiled polymer macromolecules. However, at large deformations, the polymeric molecules get stretched to accommodate the deformation; therefore, they get stiffer entropically, resulting in increased interactions between bundles, which improves the load bearing in the axial direction.

It is noteworthy here to mention the similarities between our CNT−polymer system with that of nature hierarchical structures such as bone,[12] in which a high stiffness mineral and soft matrix are mixed to obtain enhanced mechanical performance. The analogy between the two systems can be realized by comparing our material system, schematically shown in Figure 5, with the collagen matrix of bone reinforced with platelet-mineral shown in ref 12. There is a striking similarity between the mechanical functionalities of the collagen matrix (soft segment) and platelet minerals (hard segment) in bone to inherent polymer coating and CNTs in our developed material system, respectively. In both cases, the cooperative deformation mechanisms of the soft and hard segments allow for large material ductility, while in the nanoscale the material contains stiff elements. In both cases, the presence of the soft segment has a crucial role in increasing the material ductility.

Mechanical Behavior of DWNT Bundles. To identify the limits of realizable strength and energy-to-failure of our DWNT- based macroscale yarns, DWNT bundles with and without polymer coating have been tested using an *in situ* SEM tensile testing technique with a Si microfabricated cantilever as the load sensor (see Figure 6).

For analyzing the mechanical properties of DWNT bundles both the outer and inner shells of each DWNT (consistent with the analysis of the DWNT yarns) on the perimeter of the bundle was considered in calculating the true stress. Stress calculations where based on measured load and a cross-sectional area consisting of

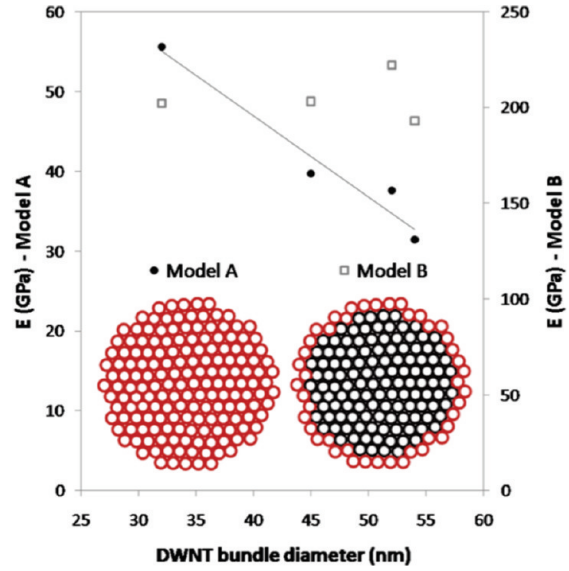

Figure 7. Diameter dependence of the experimentally determined elastic modulus for pristine DWNT bundles using two different models for calculating stress. Model A considers all DWNTs within the bundle, whereas model B only considers outer tubes.

DWNTs on the perimeter of the bundle as illustrated by model B in Figure 7. The bundles were assumed to be hexagonal close packed structures, approximately circular in geometry, consistent with TEM imaging. In nanoscale tests of individual bundles the load is applied to continuous DWNTs on the perimeter of the bundle, which span the full gauge region. The stress in the bundles was calculated using the following equations:

$$\sigma = \frac{F}{N\pi t(d_o + d_i)} \tag{3a}$$

where d_o and d_i are the outer and inner shell diameters of individual DWNTs within a bundle, respectively (2.2 and 1.6 nm). The number of load-bearing DWNTs considered within a bundle is given by

$$N = \frac{\pi(d_{bundle} - d_o)}{d_s} \tag{3b}$$

where d_{bundle} and d_s are the diameter of the entire DWNT bundle and the axes spacing of adjacent DWNTs within a bundle (2.5 nm). Equations 3a and 3b are derived in more detail in the Supporting Information. Such a model, in which only the tubes around the perimeter are considered in the cross-sectional area, is motivated by previous studies of SWNT bundles.[40] To further support this choice of model for calculating the true stress, we have investigated the diameter dependence of the elastic modulus of tested DWNT bundles. Figure 7 shows experimental results of the elastic modulus determined using two different load bearing cross sectional models for calculating stress. As expected, model B (eq 3a and 3b) in which only the outer perimeter of DWNTs are considered, is found to exhibit no variation of modulus with diameter. This is consistent with iden-

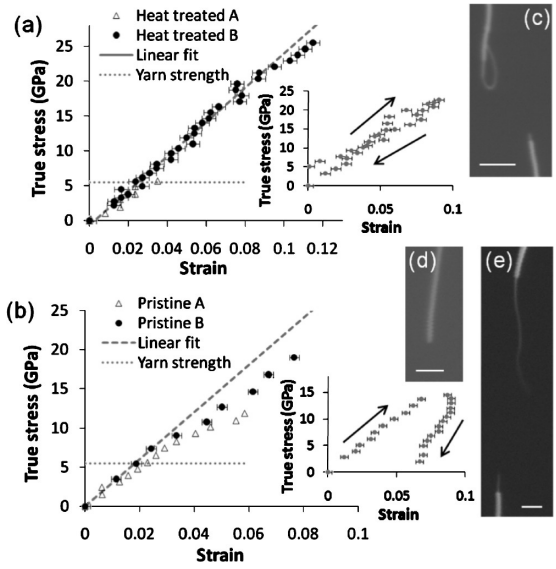

Figure 8. Stress−strain curves recorded for DWNT bundles with (a) and without (b) heat treatment. The insets show loading and unloading curves revealing plastic behavior for pristine bundles and nearly elastic behavior for heat-treated bundles. (c) Sword-in-sheath failure of heat-treated bundle. Complete fracture (d) and telescopic failure (e) of pristine bundles. All scale bars: 250 nm.

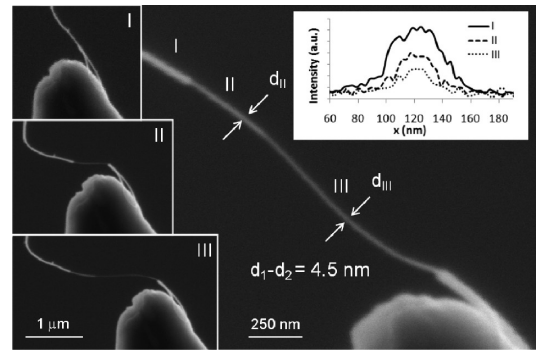

Figure 9. SEM images detailing subsequent steps (I−III) of failure of a pristine DWNT bundle. The bundle is found to fail in a telescopic manner in which inner layers of the bundle pullout with respect to outer layers. (Top right inset) SEM intensity profiles across the three different bundle layers.

tical properties of all DWNTs within the bundle and load being carried only on the outer tubes. In contrast, when model A (in which all DWNTs within the bundle are considered) is used to calculate the stress, the elastic modulus is found to decrease with diameter, which would not be expected if all DWNTs were carrying the load and had equal mechanical properties. This confirms that the best physical description of the loading conditions is that only the outer perimeter DWNTs are carrying load and that model B best describes the true stress acting on the load bearing DWNTs within the bundle.

Figure 8 shows stress−strain curves recorded from tensile tests performed on several individual bundles with and without heat treatment. Using model B to calculate true stress described earlier, the elastic modulus of DWNT bundles was found to be similar for bundles with and without polymer (*ca.* 200−250 GPa). Significant variation in the strength and failure strain was found for both heat-treated and pristine bundles. From Figure 8 it is observed that the DWNT samples fail at stresses ranging between ∼5 and 25 GPa. One distinct difference in the mechanical response of pristine and heat-treated bundles is that the pristine bundles exhibit plastic yielding consistent with a stick−slip sliding mechanism as revealed by the significant nonlinearity in the stress−strain curves after an initial elastic region. Yielding is confirmed by unloading tests on bundles near the failure stress where a large hysteresis and permanent deformation is observed in the stress−strain behavior (Figure 8B inset).

By contrast, heat-treated bundles exhibit almost purely elastic behavior before failure. Interestingly, in Figure 8, it is observed that the yield stress estimated for both heat-treated and pristine bundles is always greater than the strength of DWNT yarns when considering a consistent model for calculating stress (the experimentally determined failure strength of yarns, ∼1.4 GPa, calculated on the basis of the total cross section of DWNTs within the bundles, corresponding to a stress of ∼5.5 GPa on the outer DWNTs within a bundle). The implications of this finding with respect to failure mechanisms and energy-to-failure will be discussed in the following section and in more detail in the Supporting Information.

Two failure mechanisms have been identified in the bundles with and without polymer. In the case without polymer, the bundles are typically found to exhibit sword-in-sheath failure in which a single inner bundle of DWNTs pulls-out after fracture of the outer layers. On the other hand, bundles with polymer exhibit either telescopic pullout or complete fracture.

Sword-in-sheath failure, in the case of bundles without polymer, is revealed by high resolution SEM images of pullout of an individual inner bundle (Figure 8C) for which the difference in diameter of the inner and outer bundles after pullout (∼5 nm) is very close to 2 times the adjacent axes spacing of DWNTs within bundles (2 × 2.5 nm), suggesting the failure of a single outer layer of DWNTs in the bundle. Figure 8E and Figure 9 show telescopic failure of pristine DWNT bundles. Here the bundle is found to fail in multiple stages of pullout where a series of inner bundles slide with respect to the outer DWNTs. This difference in failure mechanism demonstrates that in the case of DWNT bundles without heat treatment, upon yielding the polymer coating introduces stronger lateral interactions between outer DWNTs and DWNTs within a bundle, leading to either complete fracture or telescopic behavior while carrying load as opposed to full

pullout of all but the outermost layer of DWNTs observed in the heat treated bundle.

DISCUSSION

High strength, high stiffness, and the ability to store and dissipate a significant amount of energy are among the most desired properties in advanced fibers. In particular, a high energy-to-failure in the relatively low strain regime of approximately 10−20% is of great interest[1,2] for many structural materials as well as in aerospace and military applications where resistance to impact and blast loadings is a vital requirement. However, even to date, concurrent advancements in all three aspects, namely strength, stiffness, and energy-to-failure, remain a nearly insurmountable challenge. This is despite the fact that we have come to realize some of nature's design principles in developing hierarchical structures with superb mechanical behavior from weak constituents and the discovery of high strength−stiffness−toughness building blocks such as CNTs. Here we have applied a novel design paradigm, merging structure and materials in the design of a hierarchical structure, resulting in enhanced mechanical properties. The yarns presented here benefit from both long-range interactions between CNT bundles, mediated by polymeric macromolecules, and direct shorter range CNT−CNT vdW interactions to carry the load and dissipate energy. The presence of hierarchy in these yarns and abundance of relatively weak interaction (entropic elasticity of polymers and vdW) resemble the structure of many biological materials.[51]

Most commercially available high performance fibers exhibit energy-to-failure in the range of 30−60 J g^{-1}, while MWNTs, of great interest as individual shells, can exhibit energy-to-failure of the order of several thousand J g^{-1} with failure strains of around 10%.[29] To date, direct spinning of SWNT and DWNT fibers have been demonstrated to exhibit energy-to-failure values similar or slightly higher compared to that of commercially available fibers such as carbon fibers and Kevlar.[2] All of the DWNT yarns with inherent polymer coatings studied in this work are found to exhibit values in the range of 30−100 J g^{-1} depending on the effective diameter of the yarns, which is comparable to that of the best available commercial fibers and directly spun CNT fibers. The energy-to-failure of our thinnest yarns with an effective diameter of ∼27 μm is 107 ± 17 J g^{-1}, which is higher than the previously reported values for similar material systems. In this regard, one may compare these values to the energy-to-failure of CNT-based yarns fabricated *in situ* CVD by Motta *et al.*, ∼60 J g^{-1},[2] to hot-drawn CNT/poly(vinylalcohol) nanocomposite yarns fabricated by Miaudet *et al.*, *ca.* 40−60 J g^{-1},[1] and to CNT yarns spun from a forest of CNTs by Zhang *et al.*, *ca.* 14−20 J g^{-1}.[3] A comparison between the mechanical behavior of CNT yarns obtained from different fabrication conditions and that of classical reinforcement fibers such as glass, kelvar, and carbon fibers is presented in a plot of specific failure energy *versus* specific strength (Figure 10). A comparison to spider silk is also included in the figure as a benchmark natural material, which exhibits high energy-to-failure in the low to moderate strain regime. Material systems which demonstrate considerable energy-to-failures only at higher strains, such as the supertough highly deformable SWNT system of Miaudet *et al.*,[1] are not discussed in this section due to their limited applications, as pointed out earlier in this section. In particular, as shown in the figure, the improved mechanical performance of our DWNT-based yarns is owed to superior ductility (∼20% strain) without compromising high strength (∼1.4 GPa) as compared to that shown in refs 1−3. In fact, a quantitative mechanistic analysis on the mechanisms of energy dissipation in pristine and heat-treated yarns (for details see Supporting Information) reveals that the major contribution to the high energy-to-failure in pristine yarns (∼100 J g^{-1}), as compared to heat-treated yarns (∼29 J g^{-1}), is a result of interactions between bundles mediated by polymer coatings molecules. In addition, for all the yarns studied here, the total energy stored in DWNTs during mechanical loading is very small (∼12 J g^{-1}). It should be noted that this is far from approaching the realizable energy-to-failure determined for individual bundles (∼520 J g^{-1}). Moreover, the stress at failure in the yarns is below the threshold to induce any permanent deformation in DWNT bundles.

On the other hand, engineering the interactions between bundles by the removal of the polymer coating and the subsequent shrinkage in the yarn diameter, which promotes vdW interactions, significantly enhances the stiffness from 26 ± 11 GPa (pristine yarns) to 67 ± 9 GPa (heat-treated yarns) with marginal improvement of the strength. However, the elimination of the long-range interactions between bundles mediated by polymer molecules and replacing them with the relatively shorter range vdW interactions (compared to polymeric interactions), results in a loss of ductility and energy-to-failure by several times.

We conclude the analysis of the energy dissipation mechanisms by noting the fact that for the small (∼2.2 outer diameter) DWNTs in the present study we do not expect, and have not observed in TEM images, the collapsed tube geometries responsible for high shear interactions reported previously.[2] It is interesting to note from Figure 10 that the heat-treated yarns reported in this study exhibit similar energy-to-failure as MWNT yarns spun directly from forests. In both cases we expect mainly vdW interactions between CNTs and do not expect collapsed CNT structures given the geometries of individual tubes within the yarns (10 nm MWNTs[3] and 2.2 nm DWNTs [this study]). In contrast, both the polymercoated yarns in this study and *in situ* CVD grown CNT yarns with collapsed geometries[2] exhibit higher

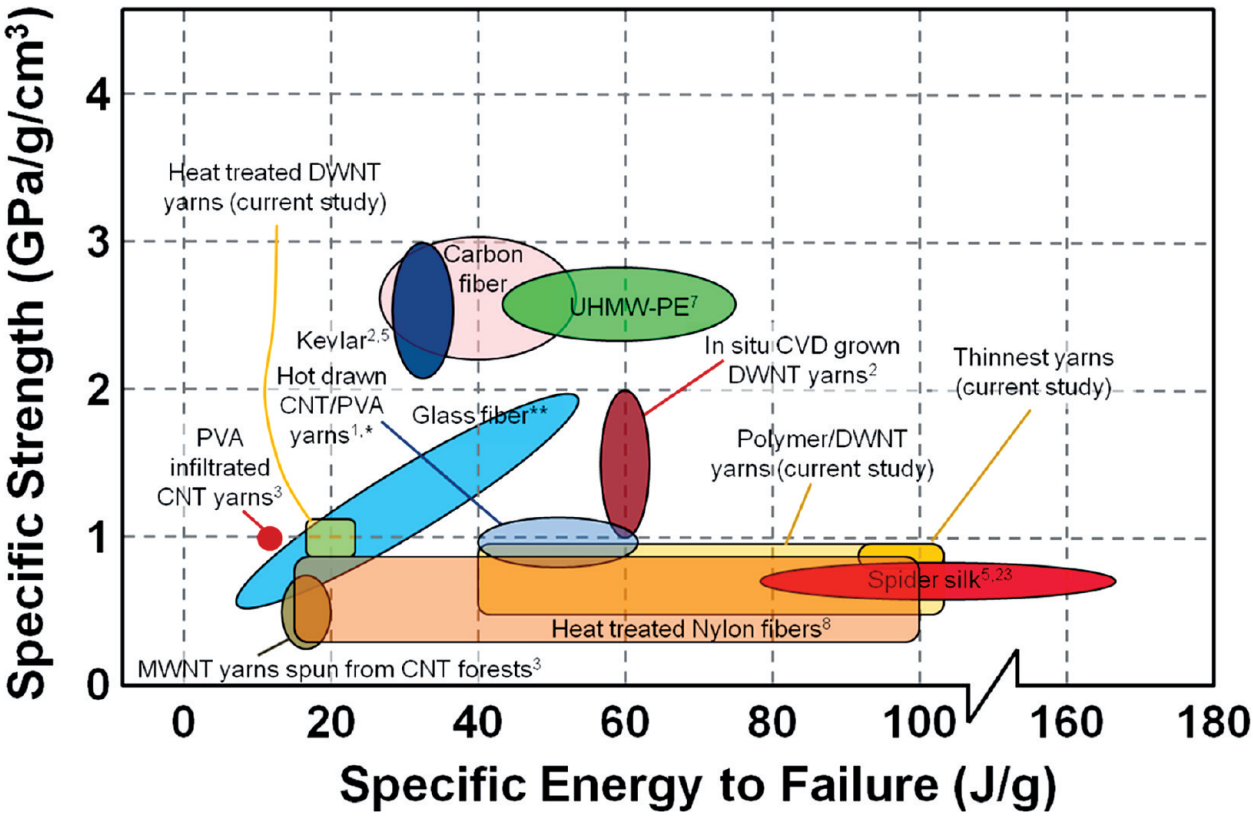

Figure 10. Specific strength as a function of specific energy-to-failure for advanced yarns and fibers.[1−8] The upper limit for the ductility of the materials presented here is taken as *ca.* 10−20% which roughly corresponds to the ductility of the spider silk at room temperature, pointing to the high energy-to-failure of a hierarchical material system in nature: (*) In this case, the density of the sample is estimated as the ratio of the area under the stress−strain curve to the reported toughness per unit mass. (**) The data for glass fibers is obtained from www.AGY.com. Results from refs 2 and 9−11 are reported only for the gage length similar to those studied here (0.8−1.3 cm) to account for the effect of material defects.

energy-to-failure presumably due to higher shear interactions between CNTs. In general, Supporting Information Table S1 demonstrates the advantages of stronger lateral interactions in CNT yarns and also suggests a more effective improvement through polymer cross-linking as compared to increased vdW interactions.

Next Generation DWNT Yarn Design. Despite the relatively high energy-to-failure and strength in our samples, our multiscale analysis identifies inefficiencies in the utilization of the individual DWNT bundles within our system given that bundles are only loaded to a small fraction of their strength. The energy analysis presented in the Supporting Information reveals that the total energy stored in CNTs is only a small fraction (~2.3%) of the total energy which can hypothetically be stored in bundles. This low ratio stems from the relatively weak lateral interactions between bundles in the current system, which does not allow for yarns to reach sufficient stress at the bundle level to dissipate more energy. In addition, more elastic energy could be stored in each bundle if the load was more effectively transferred to inner DWNTs within individual bundles to engage more DWNTs in the load transfer. Therefore, there are two key design elements in two scales that need to be addressed to maximize strength and energy-to-failure in the CNT-based yarns: (1) enhancing shear interactions between the bundles such that yarns can sustain higher loads and increase the dissipated/stored energy in each bundle (2) enhancing DWNT−DWNT interactions within each bundle to increase the load bearing cross-section.

In the current yarn system, failure occurs through the rupture of the polymer cross-linking molecules (in the case of pristine yarns) and graphitic type of shear interactions between bundles (in the yarns with no polymer). By utilizing proper polymer cross-linking, in addition to the inherent polymer coatings of the bundles, one could in principle substantially enhance the strength of the bundle−bundle lateral interactions in the yarns, thus increase the failure strength at the yarn level, and dissipate/store more energy in each bundle and in the polymer coating. This goal, for instance, could be achieved through infiltration of the yarns with stronger yet resilient polymer cross-links to simultaneously improve material strength, stiffness, and energy-to-failure. The use of polymer crosslinking represents a more tunable pathway than simply utilizing vdW interactions, the strength of which is set by the interaction between carbon atoms. Alternatively, one may induce lateral interactions between bundles by incorporating collapsed SWNTs and DWNTs. However, strain hardening mechanisms in these structures are

primarily limited to CNTs reorientation with the loading direction. Therefore, they are expected to demonstrate lower strain hardening compared to polymer infiltrated yarns. Hence, these structures are prone to localized failures at relatively low strains as can be confirmed by comparing the ductility measured in this study for pristine yarns with those of both the heat-treated yarns and the values reported for dogbone CNT morphologies or by the significant strength size effects in CVD-grown CNT yarns.[2,35]

The second design element, enhancing DWNT−DWNT interactions within each bundle, can be addressed at the sub-bundle level by the addition of cross-links between individual DWNTs. Through experiments on individual bundles, we have already demonstrated that individual bundles with a polymer coating exhibit a resistance to defects in the form of plastic yielding after the initial elastic regime, in which additional energy is dissipated after the failure of the outer DWNTs through the load transfer to the inner DWNTs by the polymer coating. Additionally, through particle radiation, shear interactions between neighboring graphitic layers can be substantially increased to raise the elastic energy stored within individual bundles. Such an approach has already been demonstrated to be effective in cross-linking shells in MWNTs[29] and SWNT bundles.[42] This step of cross-linking appears crucial to the enhancement of the mechanical behavior of the yarns. In fact, in our elastic modulus measurements of the bundles, Figure 7, the outer layer of DWNTs in each bundle carries a substantial portion of the load, leaving inner layers unutilized. In future work these possible hierarchical material design scenarios can be evaluated by applying multiscale simulation models, through which we can assess the gain in mechanical properties by implementing different material treatments and substantially narrow down the choices for effective design steps and further material developments.

One last point to mention here is that in the current state of the CNT bundle-based yarns, given the fact that the stress in the yarns even at failure is a small fraction of the strength of CNTs, the interaction between the bundles should be considered as the bottleneck which requires improvement to achieve higher strength−higher toughness materials. This can be realized by comparing the true strength of the yarns (1.4 GPa) with the average strength of the bundles, which is ~6 GPa. The latter is estimated as the ratio of the maximum force in individual bundle experiments to the cross section area of all the DWNTs within each bundle, model A in Figure 7.

CONCLUSION

The mechanical properties of high performance DWNT−polymer composite yarns, fabricated by twisting and stretching of ribbons of polymer coated DWNTs, have been measured using a multiscale *in situ* SEM experimental approach. The thinnest DWNT−polymer yarns fabricated were found to exhibit high material strength (~1.4 GPa) as well as energy-to-failure (~100 J g^{-1}), exceeding that of previously reported advanced fibers. Through *in situ* studies, at nanometer and macroscopic length scales, mechanisms contributing to energy dissipation/storage in the yarns during axial deformations were identified. Isolated DWNT bundles were found to be capable of storing/dissipating up to ~500 J g^{-1} at failure. However, the majority of the energy dissipated at failure in yarns was attributed to interactions between the polymer coating and the DWNTs, as unoptimal load transfer between individual bundles was found to prevent the stress build up in the yarns required for considerable energy storage at the bundle level. Two key design elements to further improve mechanical performance in the yarns were identified. First, tunable polymer cross-linking between DWNT bundles was proposed to increase the sustainable load transfer between bundles and the dissipated/stored energy within each bundle. Second, particle irradiation was proposed to enhance DWNT−DWNT interactions within each bundle and increase the load bearing cross-section. By addressing both these design elements, and applying multiscale models, we expect to achieve further improvements in DWNT yarns which already exhibit specific energy-to-failure superior to the best available synthetic/natural fibers.

EXPERIMENTAL DETAILS

Fabrication of DWNT Yarns. The as-produced mats are highly porous (with a density of ~0.04 g cm^{-3}), as shown in Figure 1b,c. To increase the density and to develop effective load transfer between CNT bundles, the mats were spun into yarns. For the spinning process, the CNT mats were cut into $^1/_8$, $^1/_4$, and $^1/_2$ inch wide and several inch long ribbons. Subsequently, they were twisted on a lathe machine to a few turns per millimeter of length of the ribbons. The twisting procedure was found to substantially reduce the fragility of the original mat and to turn the ribbons into fine yarns with a diameter of *ca.* 40−100 μm, as measured in SEM, Figure 1d. The twisting procedure was also accompanied by stretching the yarns at an average rate of 2−3 mm min^{-1} to induce CNT bundle partial alignment. As a consequence of the twisting and drawing of the ribbons, a tension was developed in the twisted yarn. To avoid premature rupture and prevent overloading of the yarn during stretching and twisting, a loadcell was used to monitor the applied load on the yarns. The process of twisting and stretching was continued until a tension force of ~80 mN mm^{-1} per unit width of the ribbon was generated as measured by the loadcell. Our preliminary studies on the process of twisting revealed that further stretching of the yarn resulted in the development of excessive stresses in the yarn and its failure. During spinning, oleum was sprayed on the sample which promoted sample relaxation, by allowing for the mutual sliding of bundles. After spinning, the samples were left at room temperature for a few hours to dry and reform lateral bonds between DWNTs. All DWNT yarns, and

bundles, in our study were fabricated from a DWNT mat with 14.5 wt % of polymer coating as measured using TGA. For this study, yarns were spun from ribbons with the width of $^1/_8$, $^1/_4$, and $^1/_2$ in., and the resulting effective diameters of the yarns were estimated to be 27, 38, and 53 μm, respectively.

Heat Treatment of DWNT Yarns and Bundles. To study the effect of polymeric coatings on the mechanical behavior of DWNT yarns and bundles, the coating was removed from the samples by heat treating them in two steps as follows: (1) Heat the sample in Ar to 600 °C to remove the polymeric sizing. According to TGA analysis, Figure 2, this process can remove the sizing almost entirely without damaging the CNTs. (2) Heat the sample in air to 300 °C to burn amorphous carbon which could have formed in the first step. According to TGA analysis, Figure 2, this process does not induce defects on the samples. It is to be noted that Raman spectroscopy confirms that there is no significant change in the defect density of the DWNTs as a result of the proposed heat treatment. The ratio of the intensity of the D and G peaks (I_D/I_G) in the Raman spectra before and after heat treatment is similar and very low (*ca.* 0.02−0.03), where a marginal decrease is found for the heat-treated samples suggesting that a small number of defects are annealed out. The low I_D/I_G ratio in both cases indicates that the DWNTs are of very high quality, nearly void of structural defects.[52] In the case of yarns, the process of heat treatment was performed after they were spun, since the removal of the polymers from the mats made them extremely fragile and very difficult to spin. On the other hand, for the nanomechanical experiments, the heat-treated DWNT bundles were extracted from heat-treated mats.

***In Situ* SEM Mechanical Testing of Yarns.** A microtensile tester was used, which was adapted to function inside the SEM. The stage was actuated using a linear motor at a speed of ~16 μm sec^{-1}, which corresponds to a strain rate of 1.6×10^{-3} s^{-1} for a typical gage length of 1 cm. The stage was equipped with a miniature loadcell which allowed for the measurement of tensile loads as high as 2.5 N, with a resolution of as low as 2 mN. The crosshead deformation of the sample was recorded using a linear variable differential transformer (LVDT) with a resolution of 1 μm (strain resolution of ~0.01%), which was used to calculate the average strain in the sample. All the components of the stage, the loadcell, motor, and LVDT, were vacuum compatible. Samples were gripped to the testing device using a resin-based epoxy. No sample sliding was observed during the *in situ* SEM experiments. This is consistent with the fact that, prior to sample failure in the gage sections, no sudden drops in load, which would have been suggestive of sample sliding in the grips, were observed.

***In Situ* SEM Mechanical Testing of Isolated Bundles.** A combined nanomanipulator/cantilever method was applied to test individual bundles of DWNTs which have been isolated from the as-fabricated mat material. Individual DWNT bundles, with a diameter ranging between 30 and 55 nm, were first isolated onto Cu TEM grids by lightly rubbing the grids over the bulk DWNT mat material. For each test a bundle was attached between a tungsten tip and the integrated tip of a single crystal Si cantilever using a nanomanipulator (Klocke). Manipulation was aided by electron beam etching of the DWNT bundles during the manipulation procedure.[53] The etching procedure also allowed control over the length of tested bundles. Clamping between the bundle and tips was achieved by electron beam induced deposition (EBID) of Pt.[54] Tensile tests were performed by the controlled displacement of the tungsten nanomanipulator tip (see Figure 6). The force acting on the bundle was measured using high resolution SEM images of the deflection of the Si cantilever, for which normal force constants were calibrated for each beam using a standard geometrical calibration method.[55] For each tensile test the final position of the Si tip after failure of the bundle was used to correct for any drift during testing.

Acknowledgment. H. D. Espinosa gratefully acknowledges support from ONR through award No. N00014-08-1-0108 and the ARO through award No. W911NF-09-1-0541. The authors gratefully acknowledge fruitful discussions with Dr. I. Perez. The authors also acknowledge Dr. S. Li of the Electron Probe Instrumentation Center (EPIC) at Northwestern University for obtaining TEM images and Dr. O. Compton for collection of Raman data on DWNT mats.

Supporting Information Available: The calculation of the density of CNT bundles in a hexagonally closed packed structure; estimation of the number of DWNTs carrying the load used for nanomechanical experiment on individual bundles of DWNTs; proposed method and calculations for the quantification of the mechanisms of energy dissipation and storage in DWNT yarns. This material is available free of charge *via* the Internet at http://pubs.acs.org.

REFERENCES AND NOTES

1. Miaudet, P.; Badaire, S.; Maugey, M.; Derre, A.; Pichot, V.; Launois, P.; Poulin, P.; Zakri, C. Hot-Drawing of Single and Multiwall Carbon Nanotube Fibers for High Toughness and Alignment. *Nano Lett.* **2005**, *5*, 2212–2215.
2. Motta, M.; Moisala, A.; Kinloch, I.; Windle, A. High Performance Fibres from Dog Bone Carbon Nanotubes. *Adv. Mater.* **2007**, *19*, 3721–3726.
3. Zhang, M.; Atkinson, K. R.; Baughman, R. H. Multifunctional Carbon Nanotube Yarns by Downsizing an Ancient Technology. *Science* **2004**, *306*, 1358–1361.
4. Dalton, A. B.; Collins, S.; Munoz, E.; Razal, J. M.; Ebron, V. H.; Ferraris, J. P.; Coleman, J. N.; Kim, B. G.; Baughman, R. H. Super-Tough Carbon-Nanotube Fibres—These Extraordinary Composite Fibres Can Be Woven into Electronic Textiles. *Nature* **2003**, *423*, 703–706.
5. Vollrath, F.; Knight, D. P. Liquid Crystalline Spinning of Spider Silk. *Nature* **2001**, *410*, 541–548.
6. Vigolo, B.; Penicaud, A.; Coulon, C.; Sauder, C.; Pailler, R.; Journet, C.; Bernier, P.; Poulin, P. Macroscopic Fibers and Ribbons of Oriented Carbon Nanotubes. *Science* **2000**, *290*, 1331–1334.
7. Kromm, F. X.; Lorriot, T.; Coutand, B.; Harry, R.; Quenisset, J. M. Tensile and Creep Properties of Ultrahigh Molecular Weight PE Fibres. *Polym. Test.* **2003**, *22*, 463–470.
8. Rath, J. P.; Chaki, T. K.; Khastgir, D. Change in Fiber Properties Due to the Heat Treatment of Nylon 6 Tire Cords. *J. Appl. Polym. Sci.* **2008**, *108*, 3960–3967.
9. Koziol, K.; Vilatela, J.; Moisala, A.; Motta, M.; Cunniff, P.; Sennett, M.; Windle, A. High-Performance Carbon Nanotube Fiber. *Science* **2007**, *318*, 1892–1895.
10. Motta, M.; Li, Y. L.; Kinloch, I.; Windle, A. Mechanical Properties of Continuously Spun Fibers of Carbon Nanotubes. *Nano Lett.* **2005**, *5*, 1529–1533.
11. Stano, K.; Koziol, K.; Pick, M.; Motta, M.; Moisala, A.; Vilatela, J.; Frasier, S.; Windle, A. Direct Spinning of Carbon Nanotube Fibres from Liquid Feedstock. *Int. J. Mater. Form.* **2008**, *1*, 59–62.
12. Gupta, H. S.; Seto, J.; Wagermaier, W.; Zaslansky, P.; Boesecke, P.; Fratzl, P. Cooperative Deformation of Mineral and Collagen in Bone at the Nanoscale. *Proc. Natl. Acad. Sci. U.S.A.* **2006**, *103*, 17741–17746.
13. Barthelat, F.; Tang, H.; Zavattieri, P. D.; Li, C. M.; Espinosa, H. D. On the Mechanics of Mother-of-Pearl: A Key Feature in the Material Hierarchical Structure. *J. Mech. Phys. Solids* **2007**, *55*, 306–337.
14. Jackson, A. P.; Vincent, J. F. V.; Turner, R. M. The Mechanical Design of Nacre. *Proc. R. Soc. London* **1988**, *234*, 415–440.
15. Qin, Z.; Kreplak, L.; Buehler, M. J. Hierarchical Structure Controls Nanomechanical Properties of Vimentin Intermediate Filaments. *PLoS One* **2009**, *4*, e7294.
16. Buehler, M. J.; Yung, Y. C. How Protein Materials Balance Strength, Robustness and Adaptability. *HFSP J.* **2010**, *4*, 26–40.
17. Lakes, R. Materials with Structural Hierarchy. *Nature* **1993**, *361*, 511–515.
18. Espinosa, H.; Rim, J.; Barthelat, F.; Buehler, M. J. Merger of Structure and Material in Nacre and Bone-Perspectives on *de Novo* Biomimetic Materials. *Prog. Mater. Sci.* **2009**, *54*, 1059–1100.
19. Ritchie, R. O.; Buehler, M. J.; Hansma, P. Plasticity and Toughness in Bone. *Phys. Today* **2009**, *62*, 41–47.

20. Qin, Z.; Buehler, M. J.; Kreplak, L. A Multiscale Approach to Understand the Mechanobiology of Intermediate Filaments. *J. Biomech.* **2010**, *43*, 15–22.
21. Gao, H. J.; Ji, B. H.; Jager, I. L.; Arzt, E.; Fratzl, P. Materials Become Insensitive to Flaws at Nanoscale: Lessons from Nature. *Proc. Natl. Acad. Sci. U.S.A.* **2003**, *100*, 5597–5600.
22. Mayer, G.; Sarikaya, M. Rigid Biological Composite Materials: Structural Examples for Biomimetic Design. *Exp. Mech.* **2002**, *42*, 395–403.
23. Wang, C. A.; Huang, Y.; Zan, Q. F.; Guo, H.; Cai, S. Y. Biomimetic Structure Design—A Possible Approach To Change the Brittleness of Ceramics in Nature. *Mater. Sci. Eng. C* **2000**, *11*, 9–12.
24. Verma, D.; Katti, K.; Katti, D.; Mohanty, B. Mechanical Response and Multilevel Structure of Biomimetic Hydroxyapatite/Polygalacturonic/Chitosan Nanocomposites. *Mater. Sci. Eng. C* **2008**, *28*, 399–405.
25. Meyers, M. A.; Lin, A. Y. M.; Seki, Y.; Chen, P. Y.; Kad, B. K.; Bodde, S. Structural Biological Composites: An Overview. *JOM* **2006**, *58*, 35–41.
26. Espinosa, H. D.; Juster, A. L.; Latourte, F. J.; Loh, O. Y.; Gregoire, D.; Zavattieri, P. D. Lessons in Abalone Shell Toughness Applied to Synthetic Materials. Unpublished work.
27. Yang, Y.; Chen, X.; Shao, Z.; Zhou, P.; Porter, D.; Knight, D. P.; Vollrath, F. Toughness of Spider Silk at High and Low Temperatures. *Adv. Mater.* **2005**, *17*, 84–88.
28. Locascio, M.; Peng, B.; Zapol, P.; Zhu, Y.; Li, S.; Belytschko, T.; Espinosa, H. D. Tailoring the Load Carrying Capacity of MWCNTs Through Inter-shell Atomic Bridging. *Exp. Mech.* **2009**, *49*, 169–182.
29. Peng, B.; Locascio, M.; Zapol, P.; Li, S.; Mielke, S. L.; Schatz, G. C.; Espinosa, H. D. Measurements of Near-Ultimate Strength for Multiwalled Carbon Nanotubes and Irradiation-Induced Crosslinking Improvements. *Nat. Nanotechnol.* **2008**, *3*, 626–631.
30. Haskins, R. W.; Maier, R. S.; Ebeling, R. M.; Marsh, C. P.; Majure, D. L.; Bednar, A. J.; Welch, C. R.; Barker, B. C. Tight-Binding Molecular Dynamics Study of the Role of Defects on Carbon Nanotube Moduli and Failure. *J. Chem. Phys.* **2007**, *127*, 074708.
31. Pop, E.; Mann, D. A.; Goodson, K. E.; Dai, H. J. Electrical and Thermal Transport in Metallic Single-Wall Carbon Nanotubes on Insulating Substrates. *J. Appl. Phys.* **2007**, *101*, 093710.
32. Collins, P.; Arnold, M.; Avouris, P. Engineering Carbon Nanotubes and Nanotube Circuits Using Electrical Breakdown. *Science* **2001**, *292*, 706–709.
33. Pop, E.; Mann, D.; Wang, Q.; Goodson, K.; Dai, H. Thermal Conductance of an Individual Single-wall Carbon Nanotube above Room Temperature. *Nano Lett.* **2006**, *6*, 96–100.
34. Li, Y.-L.; Kinloch, I.; Windle, A. Direct Spinning of Carbon Nanotube Fibers from Chemical Vapor Deposition Synthesis. *Science* **2004**, *304*, 276–278.
35. Stano, K. L.; Koziol, K.; Pick, M.; Motta, M. S.; Moisala, A.; Vilatela, J. J.; Frasier, S.; Windle, A. H. Direct Spinning of Carbon Nanotube Fibres from Liquid Feedstock. *Int. J. Mater. Form.* **2008**, *1*, 4.
36. Elliott, J.; Sandler, J.; Windle, A.; Young, R.; Shaffer, M. Collapse of Single-Wall Carbon Nanotubes Is Diameter Dependent. *Phys. Rev. Lett.* **2004**, *92*, 95501.
37. Dalton, A. B.; Collins, S.; Munoz, E.; Razal, J. M.; Ebron, V. H.; Ferraris, J. P.; Coleman, J. N.; Kim, B. G.; Baughman, R. H. Super-tough Carbon-Nanotube Fibres—These Extraordinary Composite Fibres Can Be Woven into Electronic Textiles. *Nature* **2003**, *423*, 703.
38. Zhang, M.; Fang, S. L.; Zakhidov, A. A.; Lee, S. B.; Aliev, A. E.; Williams, C. D.; Atkinson, K. R.; Baughman, R. H. Strong, Transparent, Multifunctional, Carbon Nanotube Sheets. *Science* **2005**, *309*, 1215–1219.
39. Liu, K.; Sun, Y. H.; Zhou, R. F.; Zhu, H. Y.; Wang, J. P.; Liu, L.; Fan, S. S.; Jiang, K. L. Carbon Nanotube Yarns with High Tensile Strength Made by a Twisting and Shrinking Method. *Nanotechnology* **2010**, *21*, 045708.
40. Yu, M. F.; Files, B.; Arepalli, S.; Ruoff, R. Tensile Loading of Ropes of Single Wall Carbon Nanotubes and their Mechanical Properties. *Phys. Rev. Lett.* **2000**, *84*, 5552–5555.
41. Yu, M. F.; Lourie, O.; Dyer, M. J.; Moloni, K.; Kelly, T. F.; Ruoff, R. S. Strength and Breaking Mechanism of Multiwalled Carbon Nanotubes under Tensile Load. *Science* **2000**, *287*, 637–640.
42. Kis, A.; Csanyi, G.; Salvetat, J. P.; Lee, T. N.; Couteau, E.; Kulik, A. J.; Benoit, W.; Brugger, J.; Forro, L. Reinforcement of Single-Walled Carbon Nanotube Bundles by Intertube Bridging. *Nat. Mater.* **2004**, *3*, 153–157.
43. Jin, H.-Z.; He, R.-R.; Zhu, J. Helicity and Inter-tube Bonding in Bundles of Single-Walled Carbon Nanotubes. *J. Electron Microsc.* **1999**, *48*, 339–343.
44. Lima, A. M. F.; Musumeci, A. W.; Liu, H. W.; Waclawik, E. R.; Silva, G. G. Purity Evaluation and Influence of Carbon Nanotube on Carbon Nanotube/Graphite Thermal Stability. *J. Therm. Anal. Calorim.* **2009**, *97*, 257–263.
45. Pang, L. S. K.; Saxby, J. D.; Chatfield, S. P. Thermogravimetric Analysis of Carbon Nanotubes and Nanoparticles. *J. Phys. Chem.* **1993**, *97*, 6941–6942.
46. Jones, N. Elastic-Plastic and Viscoelastic Behavior of a Continuous Filament Yarn. *Int. J. Mech. Sci.* **1974**, *16*, 679–687.
47. Hamm, E.; Roman, B.; Melo, F. Dynamics of Developable Cones under Shear. *Phys. Rev. E* **2004**, *70*, 026607.
48. Boudaoud, A.; Patricio, P.; Couder, Y.; Ben Amar, M. Dynamics of Singularities in a Constrained Elastic Plate. *Nature* **2000**, *407*, 718–720.
49. Leech, C. M. The Modelling of Friction in Polymer Fibre Ropes. *Int. J. Mech. Sci.* **2002**, *44*, 621–643.
50. Qian, D.; Liu, W. K.; Ruoff, R. S. Load Transfer Mechanism in Carbon Nanotube Ropes. *Compos. Sci. Technol.* **2003**, *63*, 1561–1569.
51. Buehler, M. J.; Ackbarow, T. Fracture Mechanics of Protein Materials. *Mater. Today* **2007**, *10*, 46–58.
52. Dresselhaus, M. S.; Dresselhaus, G.; Saito, R.; Jorio, A. Raman Spectroscopy of Carbon Nanotubes. *Phys. Rep.* **2005**, *409*, 47–99.
53. Yuzvinsky, T. D.; Fennimore, A. M.; Mickelson, W.; Esquivias, C.; Zettl, A. Precision Cutting of Nanotubes with a Low-Energy Electron Beam. *Appl. Phys. Lett.* **2005**, *86*, 05310-9–05310-3.
54. Agrawal, R.; Peng, B.; Gdoutos, E. E.; Espinosa, H. D. Elasticity Size Effects in ZnO Nanowires—A Combined Experimental–Computational Approach. *Nano Lett.* **2008**, *8*, 3668–3674.
55. Meyer, E.; Hug, H.; Bennewitz, R. *Scanning Probe Microscopy: The Lab on a Tip;* Springer-Verlag: Berlin, 2004.